Biophys Rep 2018, 4(3):133–142
https://doi.org/10.1007/s41048-018-0051-5

Biophysics Reports

METHOD

Three-dimensional electron spin resonance imaging of endogenous nitric oxide radicals generated in living plants

Yuanlin Cao[1]✉, Yongsheng Chen[1], Qian Wan[1], Jungai Hu[1], Baolu Zhao[1]✉

[1] Institute of Biophysics, Chinese Academy of Science, Beijing 100101, China

Received: 28 March 2017 / Accepted: 15 May 2017 / Published online: 9 May 2018

Abstract Electron spin resonance imaging (ESRI) has been developed to detect the spatial contribution of free radicals in recent years, but all of these studies are used in animal systems and almost of them using exogenous spin probes and only a few to study the endogenous free radicals in vivo. However, there is no report about the endogenous free radical three-dimensional (3D) EPRI in plant because of low concentration of endogenous free radicals and low resolution of the L-band ESRI. Recently, we have developed the imaging resolution better than 200 μm which is higher 10 times than L-band (about 1–3 mm) and the sensitivity is higher about 1000 times than that of L-band ESRI. Using this system and spin trapping technique, we studied spatial contribution of the endogenous nitric oxide (NO) radical generation in wheat leaves and got a clear 3D ESRI picture and CT (computed tomography) of NO of a wheat leaf. This imaging picture shows a clear spatial distribution of NO free radicals in the leaf. This is the first 3D ESRI of endogenous NO free radical generated in plant in the world. We have also studied the distributions of NO generation in different plants from different species with different shapes and it is shown that this is a convenient method to study the endogenous free radicals in plants.

Keywords Electron spin resonance (ESR), Electron spin resonance imaging (ESRI), NO free radicals, Plant

INTRODUCTION

Electron spin resonance (ESR) is the most direct and effective technique to detect free radicals, but it can only give the information about the free radical's kind and concentration. Electron spin resonance imaging (ESRI) is a representation of the spatial distribution of the ESR intensity or other parameters in a heterogeneous sample, and it has been developed in recent years, especial ESR instrument operating at low frequencies has made it possible to detect free radical spatial contribution in animals (Fu *et al* 2014; Kobayashi *et al*. 2014; Lin *et al*. 2014; Morosan *et al.* 2015; Zou and Zhang 2017). Because of the low concentration and short life time of natural free radical in biological bodies, the extraneous spin probes have been used in most ESRI experiments. Nitroxide stable free radicals exhibit varied chemical and biological properties and their biological applications have been greatly expanded over the past few years (Maeda 2012, 2013). They can serve as *in vivo* functional imaging probes that non-invasively report on the oxygen status and redox properties in different tissues, such as tumors (Berliner *et al*. 1987; Feng *et al*. 2016; Hou *et al*. 2005; Mikuni *et al*. 2004; Matsumoto *et al*. 2006), heart (Kuppusamy *et al*. 1994; Zweier *et al*. 1998), brain (Hiramatsu *et al*. 1995; Kuppusamy *et al*. 1995a, b; Ueda *et al*. 1997; Velayutham *et al*. 2003), and liver (Yoshimura *et al*. 1995). It was also used to detect the physical state of plant (Berliner and Fujii 1985). There are a few studies on the endogenous free radicals generated *in vivo* in physiological condition using L-band ESRI (Yokoyama *et al*. 1996, 1997, 2000, 2002), but no any report about the endogenous free radicals generated in plant using this technique because of low

✉ Correspondence: Caoyl@moon.ibp.ac.cn (Y. Cao), Zhaobl@ibp.ac.cn (B. Zhao)

concentration of endogenous free radicals and low resolution of the L-band ESRI.

Nitric oxide (NO) is now recognized to play an important physiological role in animals either as a regulator, involved in signal transduction mechanisms, or as a toxic or protective molecule depending on the concentration and the tissue where it is acting (Feng *et al*. 2016; Gao *et al*. 2016; Millar and Day 1997; Wendehenne *et al*. 2001; Wink *et al*. 1997; Zhao 2015). In plants, although NO research is more recent than in animal, mounting evidences suggest that NO plays important roles in diverse physiological processes such as growth and development (Laxalt *et al*. 1997), plant disease resistance (Noritake *et al*. 1996), abiotic stress (Delledonne *et al*. 1998), and signal transition (Durner *et al*. 1998).

We have developed ESR spin trapping technique (Zhang *et al*. 2001; Zhou *et al*. 1999) to study NO free radicals generated during development (Zhang *et al*. 2002, 2004), ischemia–reperfusion heart (Shen *et al*. 1998; Zhao *et al*. 1996a, b), and brain (Zhang *et al*. 2004a, b), inflammation Li *et al*. 2000; Zhao *et al*. 1996a, b), neurodegenerative diseases (Guo *et al*. 2005; Zhao 2005) and protective effects of natural antioxidants (Shen *et al*. 2000). We have also developed this method (Cao *et al*. 2005; Xu *et al*. 2004, 2005) to study the NO free radical generated from plant (Xu and Zhao 2003) and role of endogenous NO burst in the resistance of wheat to stripe rust (Guo *et al*. 2004). We have developed an L-band ESRI system and got a clear picture of baby mouse by spin probe (Wu *et al*. 2005, 2007). In this study, we have developed an X-band ESRI system and studied the endogenous NO distribution in wheat leaves and got a clear three-dimensional (3D) picture of NO and CT (computed tomography) of a wheat leaf. We also studied the distributions of NO generation in different plants with different shapes. This is the first 3D ESRI of endogenous NO free radicals in plant until now and can be used in the future study as a strong and convenient technique.

RESULTS

Stable of the ESR signal of NO spin trapped by $(MGD)_2$–Fe^{2+} and $(DETC)_2$–Fe^{2+}

Complex

Figure 1A shows a standard curve of $(MGD)_2$–Fe^{2+}–NO complex obtained from the reaction of NO solution with $(MGD)_2$–Fe^{2+}. Inset in Fig. 1A is a three-line ESR signal (g = 2.035, aN = 1.27 mT) of $(MGD)_2$–Fe^{2+}–NO obtained after MGD and Fe mixed with authority NO (certain concentrations of NO gas). Figure 1B is a series of ESR signal of $(MGD)_2$–Fe^{2+}–NO with good S/N three-lines obtained from a wheat leaf after wheat is cultured in a MGD and Fe^{2+} solution and the signal is increased continuously until 2 h, then keeps on a plateau, after 4 h, the signal continuously decreased (Fig. 1C) and it can be detected after 24 h. When the wheat leaf is cut off from the wheat, the signal will continuously decrease but be stable during 30 min (Fig. 1D, E) (it takes about 30 min to collect the data for ESRI). In the presence of NO inhibitors, PTIO (2-phenyl-4, 4,5,5-tetramethylimidazoline-1-oxyl) or NMMA (N^G-monomethyl-L-arginine), the signals decreased (result not shown), indicating that this signal was generated, at least part, by the endogenous NO free radicals from the pathway of L-arginine. Figure 1E shows a decay curve of $(DETC)_2$–Fe^{2+}–NO complex obtained from the wheat leaf absorbed DETC and Fe^{2+} solution respectively. Inset in Fig. 1E is a ESR spectrum of $(DETC)_2$–Fe^{2+}–NO complex. It is found that the signal of $(MGD)_2$–Fe^{2+}–NO is better and more stable than that of $(DETC)_2$–Fe^{2+}–NO. So $(MGD)_2$–Fe was used to spin trap the endogenous NO generated in the plants in this paper.

Imaging resolution

The imaging resolution achieved by this X-band ESRI system was determined by two capillaries containing carbon powder as shown in Fig. 2. The two samples spaced apart at a distance of 500 μm, center to center, and 125 μm, edge to edge. Figure 2A shows the schematic diagram of position and sizes of the detected samples. Figure 2B shows the partial slice images of ESR–CT; Fig. 2C shows the stacked 3D ESR–CT imaging, and Fig. 2D shows the 3D spatial image of the phantom. The image clearly identifies the two samples. This means that the imaging resolution obtained with our developed ESRI system is better than 200 μm.

ESRI of NO free radical generated from the wheat leaf and auricle

Figure 3 shows a typical set of ESRI images in the wheat leaf after the absorption of a solution containing Fe^{2+} and MGD. Figure 3A shows two-dimensional (2D) ESRI images of spin density in the cross section (ZX-plane) of endogenous NO free radical generated in the wheat leaf. Figure 3D shows a 3D spatial image of endogenous NO free radical in a wheat leaf. Figure 3B, C shows partial slice and slice stacked images of ESR–CT from Fig. 3D, respectively. It can be found that the strongest signal of NO free radical is located in the leaf vein.

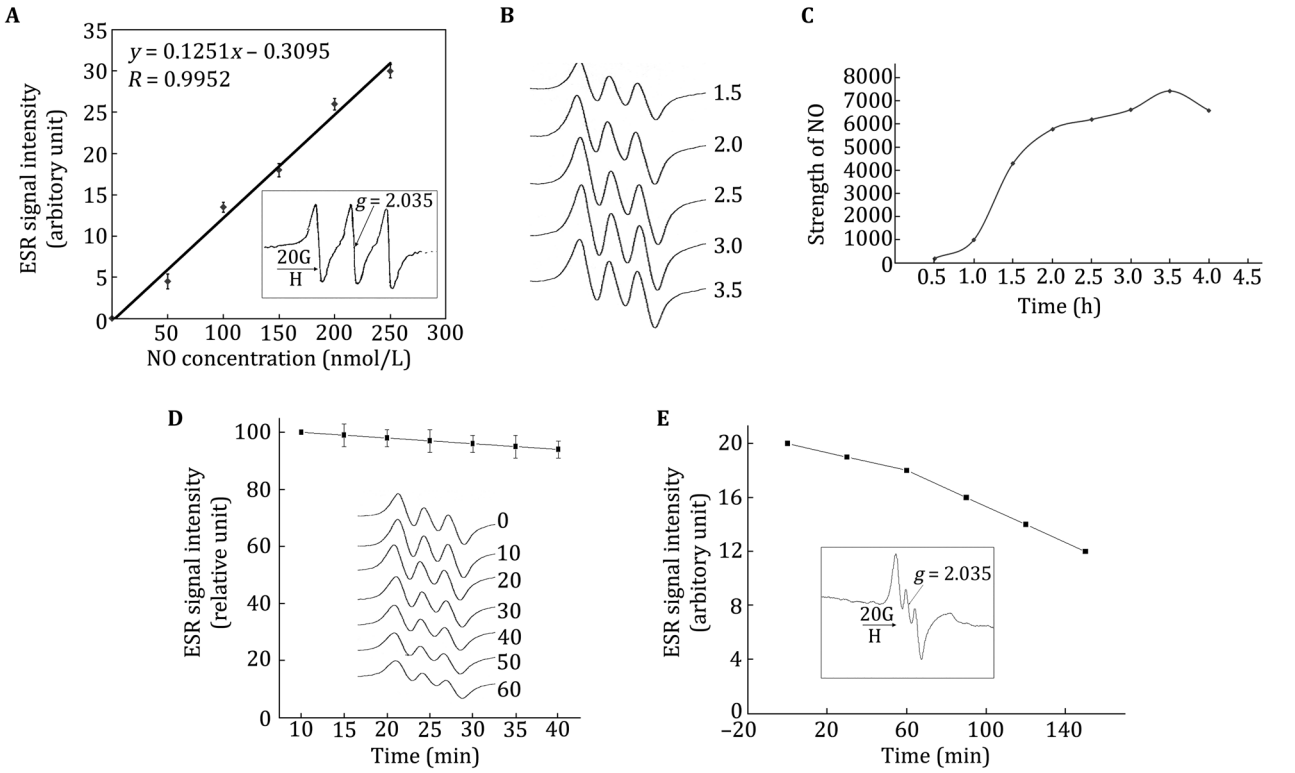

Fig. 1 **A** Standard curve of the $(MGD)_2$–Fe^{2+}–NO complex which was obtained by the reaction of authority NO solution with $(MGD)_2$–Fe^{2+}, as described in "Materials and methods" section. Inset is the ESR spectrum that represents NO concentration at 500 nmol/L. **B** ESR spectra of $(MGD)_2$–Fe^{2+}–NO complex generated in live wheat leave. **C** The accumulation of $(MGD)_2$–Fe^{2+}–NO complex generated in live wheat leave with time. **D** The decay curve of ESR signal of $(MGD)_2$–Fe^{2+}–NO complex generated in live wheat leave with time. Inset is the ESR spectra of $(MGD)_2$–Fe^{2+}–NO complex generated in live wheat leave with time. **E** The decay of ESR signal of $(DETC)_2$–Fe^{2+}–NO complex generated in live wheat leave with time, the inset is an ESR spectrum of $(DETC)_2$–Fe^{2+}–NO complex generated in live wheat leave. The ESR conditions: X-band, microwave power 5 mW, Modulation 4G, room temperature

Figure 4 shows a typical set ESRI images in the wheat auricle after the absorption of a solution containing Fe^{2+} and MGD. Figure 4A shows 2D ESRI images of spin density in the cross section (ZX-plane) of endogenous NO free radical generated in the wheat auricle. Figure 4D shows a 3D spatial image of the NO free radical. Figure 4B, C show partial slice and slice stacked images of ESR–CT from Fig. 4D, respectively. It can be found that the shape of the auricle is different from the leaf but the strongest signal of NO is also located in the leaf vein.

ESRI of NO free radical generated from millet grain and bud

Figure 5 shows the 3D ESRI images at different visual angles of the millet grain and bud after absorption of a solution containing Fe^{2+} and MGD (Fig. 5A–C), and a partial slice images of ESR–CT (Fig. 5D). 3D ESRI images were successfully reconstructed only for those grain and bud with $(MGD)_2$–Fe^{2+}–NO. There is no signal can be found in the dry grain and the grain incubated in water before sprouting. The NO signal can only be detected in the sprouting grain with spin trapping. It can be found that the strongest signal of NO is located in the bud and the signal of NO is over whole grain.

ESRI imaging of the NO free radicals generated from forsythia young stem

Figure 6 shows a typical set ESRI images in the forsythia young stem after the absorption of a solution containing Fe^{2+} and MGD. Figure 6A shows the 2D ESRI images of spin density in the cross section (*ZX*-plane) of endogenous NO free radical generated in the forsythia young stem. Figure 6D shows a 3D spatial image of the NO free radical in the forsythia young stem. Figure 6B, C show partial slice and slice stacked images of ESR–CT from Fig. 6D, respectively. It can be found that the shape of the forsythia young stem is different with the wheat leaf and auricle and the strongest signal of NO is located in the best.

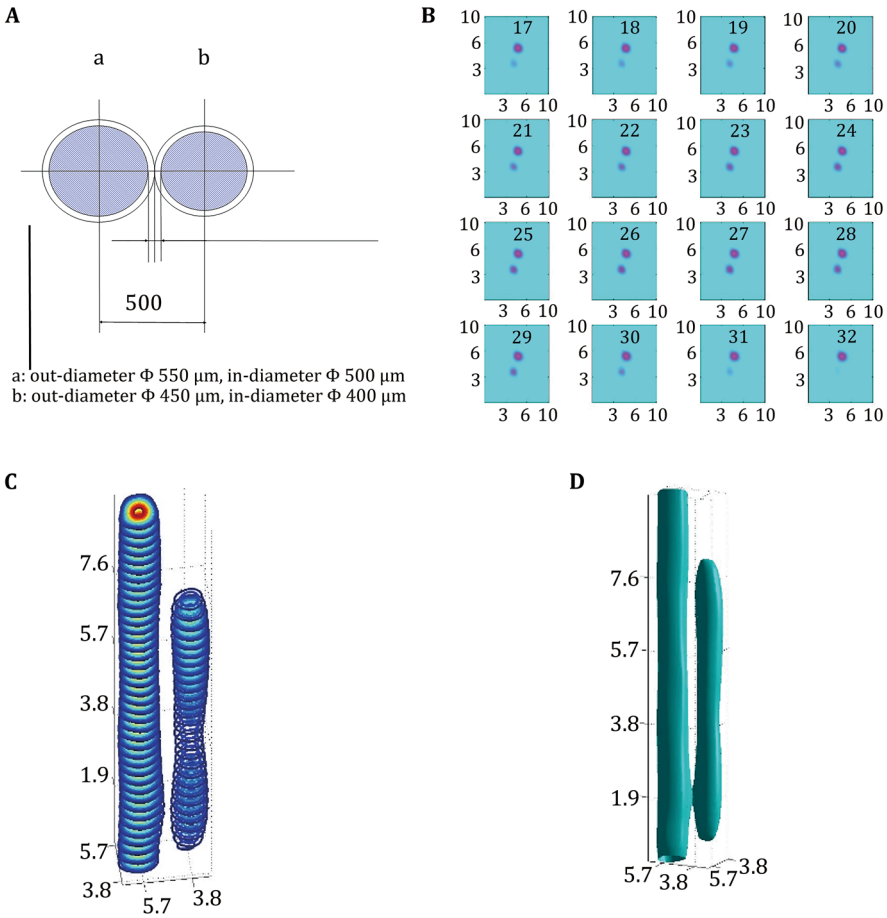

Fig. 2 Images of phantom for resolution detection. **A** Schematic diagram of cross-sectional view and sizes of the detected samples. **B** Partial slice images of ESR–CT. **C** Stacked ESR–CT 3D image. **D** 3D spatial image of the phantom. Sample: carbon power. Data acquisition parameters: projections 9 × 9, scan time 40 s, sweep width 50 G, microwave power 5 mW, modulation amplitude 2.5 G, gradient field 82 G/cm, room temperature

DISCUSSION

In plants, NO serves as a signal in hormonal and defense responses (Dangl 1998; Lancaster 1994; Neill *et al*. 2003; Stohr and Ullrich 2002). NO also plays an important role in plant growth elongation (Gouvea *et al*. 1997; Leshem and Haramaty 1996), and activation of some enzymes for plant cell differentiation (Ferrer and Ros Bareclo 1999). There are evidences about the regulation of NO on plant maturation and senescence (Leshem *et al*. 1998). NO treatment inhibits the production of ethylene which inducing plant ripening and aging (Leshem *et al*. 1998). NO induces the production of phytoalexins which promote plant growth and inhibit senescence (Millar and Day 1997). NO also plays an important role in activities of pathogen-related (PR) protein-phenylalanine ammonia-lyase (PAL) and restriction of multiple pathogens. NO functions as a signal in plant disease resistance for hypersensitive necrotic reaction (Van Camp *et al*. 1998), production of phytoalexins (Chandok *et al*. 2004), expression of defence gene (Zeidler *et al*. 2004), increase of chlorophyll (Leshem and Haramaty 1996). To understand the roles and mechanisms of NO in the plant, it is first important to know where NO is produced and contributed in plant.

To examine the location and contribution of NO in biological system, the available techniques without invasiveness used in practice are EPR imaging and fluorescence and luminal-chemiluminescence imaging (Leshem and Pinchasov 2000). Nagano and Yoshimura reviewed the background and current status of imaging techniques for approach on biological NO, *i.e.*, bioimaging of NO, with emphasis on the imaging techniques that utilize EPR spectrometry and fluorometry (Nagano and Yoshimura 2002).

EPR imaging is considered to be the most effective technique available for non-invasive observation of the spatial distribution of free radicals. Over the past decade, EPR spectroscopic methods combined with NO-trapping techniques have emerged as important tools and have provided much important information about the roles of NO in biological system. The organs or tissues with a locally high, pathological level of NO can be targets, so that this method was used to detect the NO generation in pathophysiological conditions involving the overproduction of NO, such as from the head and abdomen of LPAs stimulated mouse (Suzuki *et al*. 1999),

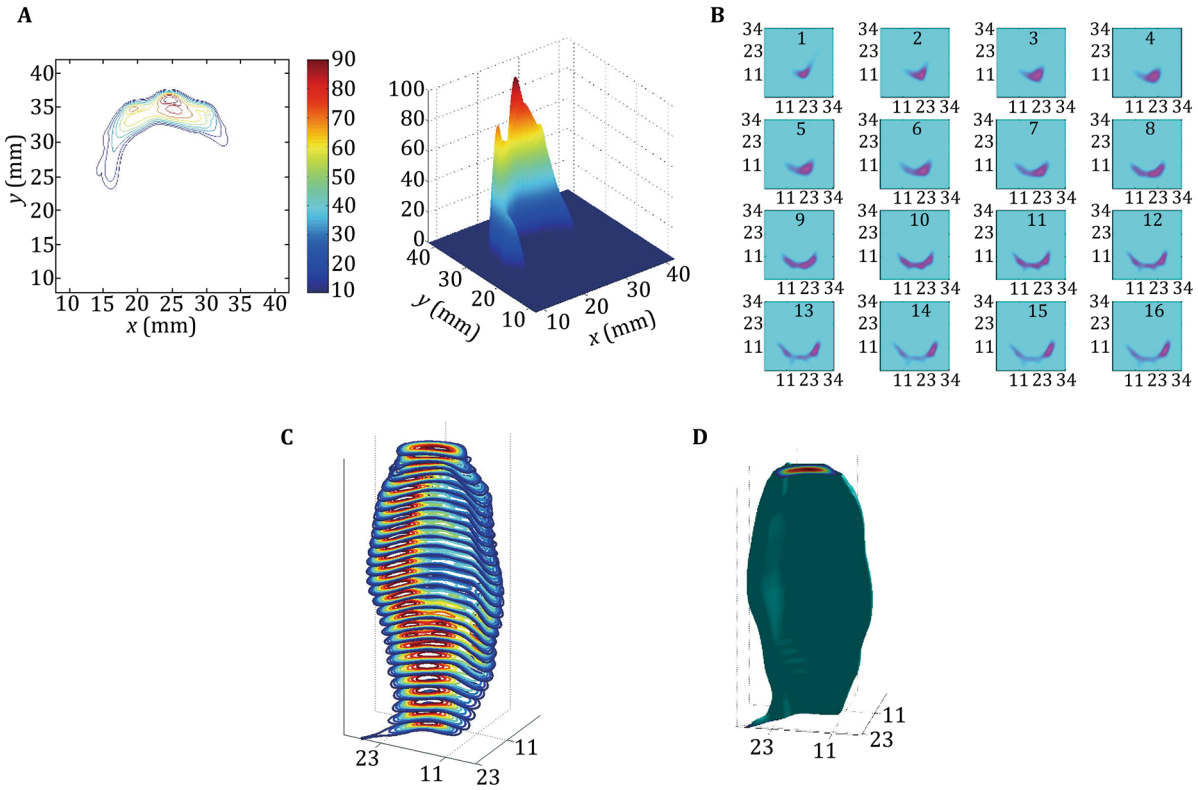

Fig. 3 ESRI images in the wheat leaf after the absorption of Fe and MGD, respectively. **A** Contour and distribution images of spin density. **B** Partial slice images of ESR–CT. **C** Stacked image of ESR–CT. **D** 3D spatial image. The ESR conditions: X-band, microwave power 2 mW, modulation amplitude 1 G, gradient field 90 G/cm, and room temperature

rat brain during ischemia-hypoxia. EPR images from the frozen resected brain were obtained by employing an $(DETC)_2$–Fe^{2+} trap and an EPR imaging system with a microwave frequency of 1.2 GHz (Kuppusamy *et al*. 1995a, b, 1996), the endogenously produced NO in the abdominal region in a LPS-induced sepsis model mouse by using an $(DTCS)_2$–Fe^{2+} complex as an NO trap (Kuppusamy *et al*. 1994); an imaging of nitric oxide generation during ischaemia was performed with the use of ^{15}N isotope labeling; it was possible to map the metabolic pathway of this nitric oxide generation (Zweier *et al*. 1998). However, *in vivo* EPR imaging is not applicable to physiological levels of NO in plant because of the low concentration of NO generated in the biological system and limitations of currently available L-band EPR instrumentation (low resolution).

There is no any report about the EPRI of animal using X-band instrument, since at conventional X-band (9–10 GHz) frequencies water-rich samples have a high dielectric loss which reduces the *Q*-factor of the resonant cavity and small size of the cavity, it is difficult to be used in EPRI for animal tissues. In the other hand, these two characters X-band EPR are suitable for plant with lower concentration of water and smaller size of plant tissues.

Fluorescent indicators for bioimaging of NO have been applied to various biological samples to examine production of NO. The most widely used fluorescent indicators for detecting intracellular NO are DAFs and DARs, which can permit the measurement of NO production in various living cells, tissues, and specimen. Leaves and callus of *Kalanchoe daigremontiana* and *Taxus brevifolia* were used to investigate NO induced apoptosis in plant cells (Pedroso *et al*. 2000a). The NO burst preceded a significant increase in nuclear DNA fragmentation and cell death. L-NMMA significantly decreased NO production and apoptosis in both species. Pedroso *et al*. (2000a) concluded that NO is involved in DNA damage leading to cell death and proposed a potential role of NO as a signal molecule in these plants. Foissner *et al*. (Pedroso *et al*. 2000a, b) used 5-diaminofluorescein diacetate (DAF-2 DA), in conjunction with confocal laser scanning microscopy, for *in vivo* real-time imaging of an elicitor-induced NO burst in tobacco. A growing body of evidence suggests that NO, an important signaling and defense molecule in mammals, plays a key role in activating disease resistance in plants, acting as a signaling molecule and possibly also as a direct antimicrobial agent. The results revealed additional similarities between the plant and the animal hosts responsing to infection. Endogenous NO production

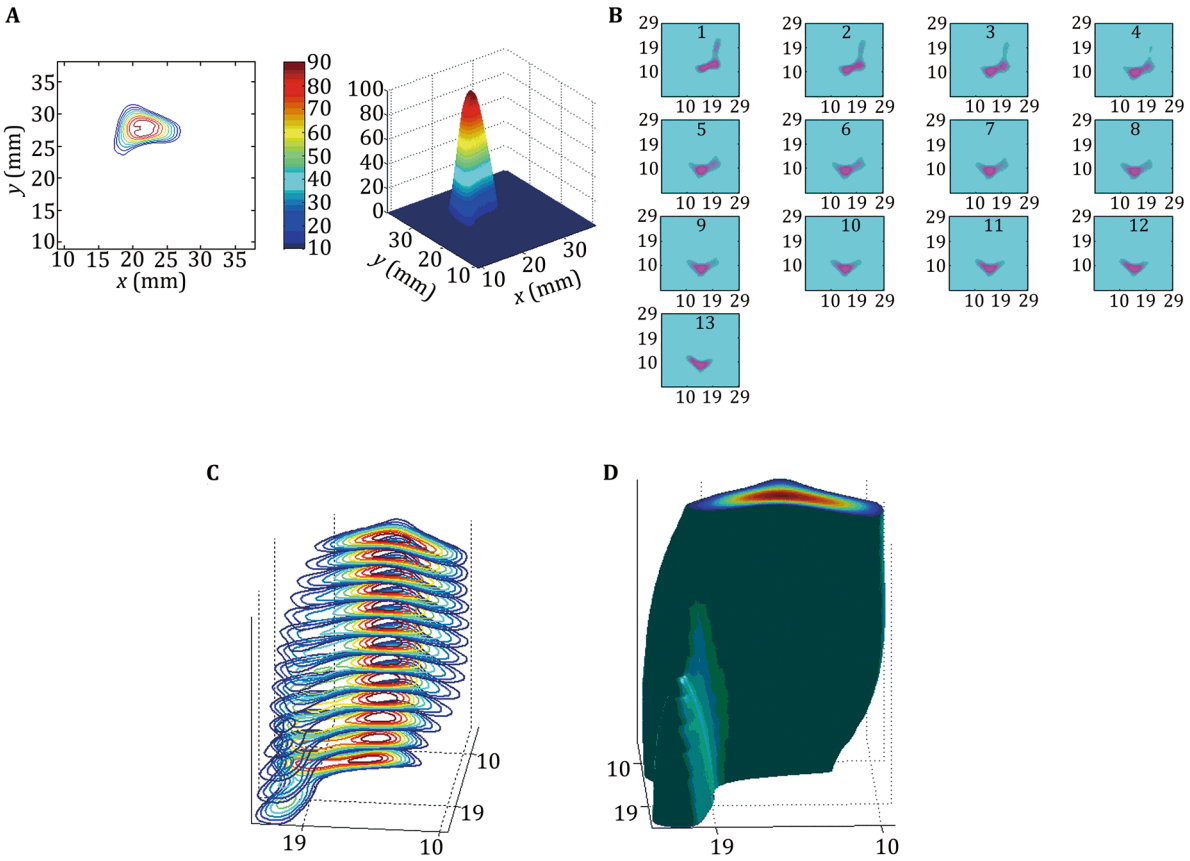

Fig. 4 ESRI images in the wheat auricle after the absorption of Fe^{2+} and MGD, respectively. **A** Contour and distribution images of spin density. **B** Partial slice images of ESR–CT. **C** Stacked image of ESR–CT. **D** 3D spatial image of endogenous nitric oxide free radical generated in a wheat auricle. The ESR conditions: X-band, microwave power 2 mW, modulation amplitude 1 G, gradient field 90 G/cm, and room temperature

was examined in roots by comparing wild-type and mutant seedlings loaded with the permeable NO-sensitive dye fluorophore DAF-2 DA. It was found that NO production in plants, which is the strongest at the root tip of young seedlings when roots were treated with 50 μmol/L abscisic acid (ABA), could be inhibited by L-NAME. To address the role of *AtNOS1* in stomates, NO production and stomatal closure in epidermal peels from wild-type and *Atnos1* plants were compared. ABA-induced NO production (measured as increased fluorescence of the NO-sensitive dye DAF-2 DA) was severely inhibited in *Atnos1* guard cells compared with wild-type and rescued (expressing AtNOS1) mutant lines (Guo *et al*. 2004). This technique was also successfully used to study the NO free radicals in endothelial cell (Kojima *et al*. 1999), smooth muscle cell (Itoh *et al*. 2000; Kojima *et al*. 1998a, b), bone marrow stromal cell (Gorbunov *et al*. 2000) and the regulation of ion channel (Ahern *et al*. 2000) and process of inflammation (Lopez-Figueroa *et al*. 2000a), even in mitochondria (Lopez-Figueroa *et al*. 2000b), ritina (Blute *et al*. 2000) and bran slices (Kojima *et al*. 1998a, b) and small animal drosophila (Yermolaieva *et al*. 2000) and plant cell of leaves and callus. The concentration and resolution limitation of fluorescence imaging for NO is about nmol/L and nm, which is suitable for the study of NO imaging in cell and sub-cell. However, it is difficult to image the special distribution of NO in larger scale about μm–mm such as in the leaves of plant by fluorescence confocal laser microscopy. The X-band EPRI is just suitable to image the NO generated in such scale of plant tissues.

We have studied the generation and spatial contribution of NO free radicals in different plants with different shapes from different species, wheat leaves and auricle, grain and bud, forsythia young stem.

MATERIALS AND METHOD

Materials and apparatus

Wheat seeds (*Triticum aestivum* L. cv. Hanxuan 10) and grain obtained from Northwest Science and Technology University of Agriculture and Forestry were sown in

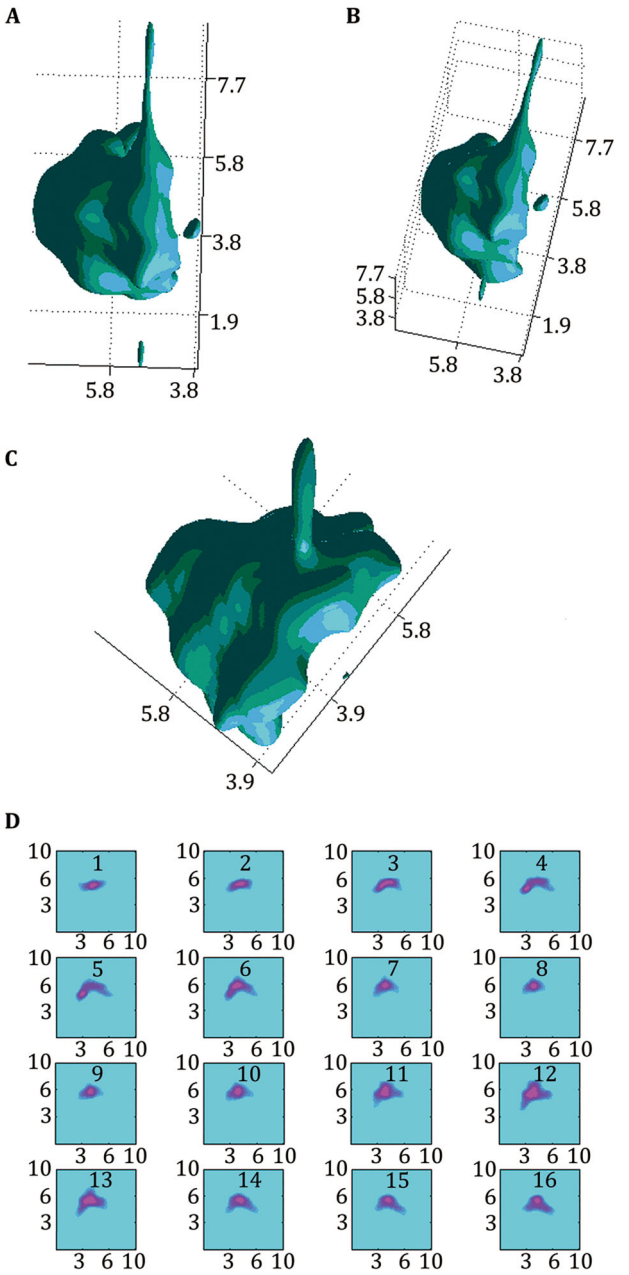

Fig. 5 ESRI images of NO free radical generated from millet gain and bud (after the absorption of Fe and MGD, respectively) during germinating. **A–C** 3D images at different visual angles. **D** Partial slice images of ESR–CT. The ESR conditions: X-band, microwave power 2 mW, modulation amplitude 1 G, gradient field 90 G/cm, room temperature

plastic pots and irrigated with Hoagland's solution. The seeds were allowed to germinate and develop in the greenhouse. The growth chamber was set at a relative humidity of 60%–80%, day/night temperatures of 25/20 °C, 14-h photoperiod (600 mol quanta/m^2·s PAR) supplied by fluorescent lamps and 10-h dark. Six-day-old seedlings and germinating grains were used as experimental materials.

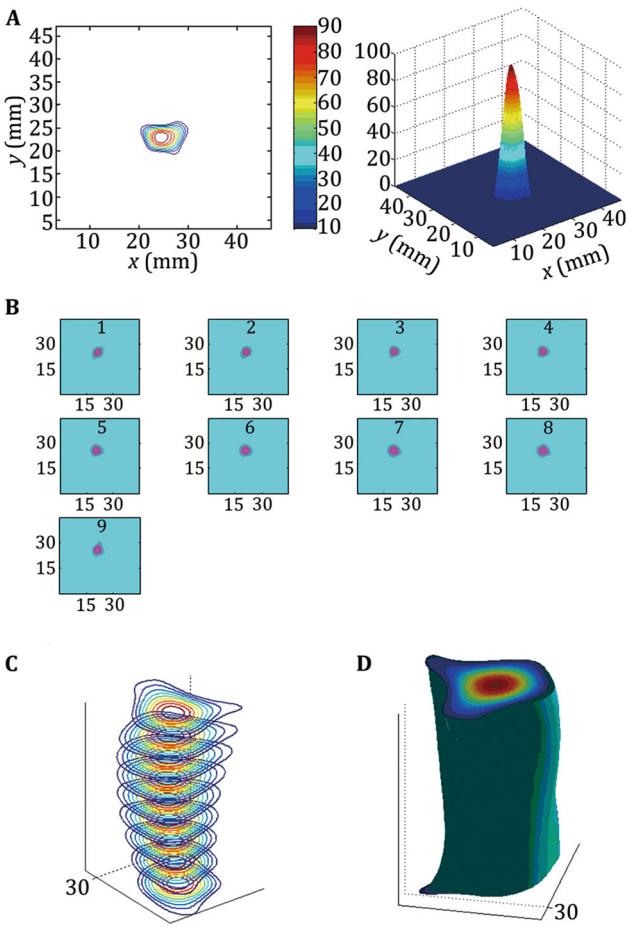

Fig. 6 ESRI images in the forsythia young stem after the absorption of Fe and MGD, respectively. **A** Contour and distribution images of spin density. **B** Partial slice images of ESR–CT. **C** Stacked image of ESR–CT. **D** 3D spatial image of endogenous nitric oxide free radical generated in a forsythia young stem. The ESR conditions: X-band frequency, microwave power 2 mW, modulation amplitude 1 G, gradient field 90 G/cm, room temperature

DETC (diethyldithiocarbamate), MGD (*N*-methyl-D-glucamine dithiocarbamate), L-NMMA (N^G-monomethyl-L-arginine), and PTIO (2-phenyl-4,4,5,5,-tetramethylimidazoline-1-oxyl 3-oxide) were purchased from Sigma Chem. Co.. All other reagents purchased in China were analytical grade.

ESR experiments were performed on a BRUKER 200D-SRC spectrometer (Germany). The $(DETC)_2$–Fe^{2+}–NO and $(MGD)_2$–Fe^{2+}–NO complex both in solution and in intact leaves was measured, respectively, in a 2.5-mm internal diameter quartz tube at 25 °C. The conditions for measurement were X-band, 100 kHz modulation with 3.2 G amplitude, microwave power 20 mW, central magnetic field 3385 G, scan width 400 G, time constant 0.3 s, scan time 4 min. The whole height of triplet hyperfine structure, namely the peak at g = 2.035 and

its two neighbor peaks, was taken as relative intensity of the ESR signal.

Spin trapping NO in plants

Six-day-old wheat seedlings were treated according to following procedure; seedlings were transferred to a culture medium containing 15 mmol/L $FeSO_4$ and 40 mmol/L MGD, but for DETC, it was brushed on the leaves. 24 h later, the leaf discs or auricle were inserted directly into a quartz tube to determine NO on an ESR spectrometer. The forsythia young stem was inserted directly into a culture medium containing 15 mmol/L $FeSO_4$, and 40 mmol/L MGD solution for 5 h then transferred into a quartz tube to determine NO on an ESR spectrometer. In the experiment germinating of grain, the grain was incubated at the temperatures 18 °C and then the germinating grains were transferred to a culture medium containing 15 mmol/L $FeSO_4$, and 40 mmol/L MGD solution. 7 h later, the grain was inserted directly into a quartz tube to determine NO on an ESR spectrometer.

ESR imaging system

The X-band ESR Imaging (ESRI) system developed at our laboratory includes a set of X-band EPR spectrometer modified Varian type E-109, a pair of three-dimensional gradient magnetic field coils, and a PC microcomputer-based data system. The operation frequency range of the EPR spectrometer is at 8.8–9.6 GHz, using a rectangular TE_{102} mode cavity with 100 kHz field modulation. The 3D gradient coils were plate form coils that processed using whole copper plates instead of the wound with copper wires, which made its structure so compact that it was much thinner and smaller comparing to those traditionally used in ESRI. A maximum gradient strength of up to 9 mT/cm could be obtained with driving current of about 60A in each dimension coil. The spatial linearity was better than 3% in all three dimensions within a cubic volume range of 10 mm × 10 mm × 10 mm.

Projection data acquisition and subsequent image reconstruction were performed using PC computer equipped a data acquisition card with D/A and A/D converters of 12 bit. A software package of application programs was written with Matlab which handles auto-processing of spectra data and reconstruction of ESRI spatial imaging by the filtered back-projection method.

In vivo ESR measurement and ESR-imaging

After 40-min absorption by $FeSO_4$ and MGD, the leaf was positioned in the TE_{102} cavity with its leaf axial along to the *Y*-direction of gradient field. The ESR spectrum with a zero-field gradient was measured first, a group of total 9 × 9 projection spectra were acquisitioned at gradient strength of 2.7 mT/cm with the gradient direction rotating in an angle increment of 20°. Using 40-s scans, the total time for data acquisition was approximately 60 min. Before image reconstruction, spectra were processed as follows: noise filtering, baseline correcting, double integrating, and resolution enhancement by convolution difference technique. The processed spectra were then used as projection for the 3D image reconstruction using two-stage back-projection reconstruction algorithm. To avoid some artifacts in the image, a filtering process to the image was carried out before plotting. In this process, the standard deviation of the image was subtracted from each element of the image.

Compliance with Ethical Standards

Conflict of interest Yuanlin Cao, Yongsheng Chen, Qian Wan, Jungai Hu, and Baolu Zhao declare that they have no conflict of interest.

Human and animal rights and informed consent This article does not contain any studies with human or animal subjects performed by any of the authors.

References

Ahern GP, Hsu SF, Klyachko VA, Jackson MB (2000) Induction of persistent sodium current by exogenous and endogenous nitric oxide. J Biol Chem 275:28810

Berliner LJ, Fujii H (1985) Magnetic resonance imaging of biological specimens by electron paramagnetic resonance of nitroxide spin labels. Science 227:517

Berliner LJ, Fujii H, Wang X, Lukiewicz SJ (1987) Feasibility study of imaging a living murine tumor by electron paramagnetic resonance. Magn Reson Med 4:380–384

Blute TA, Lee MR, Eldred WD (2000) Direct imaging of NMDA-stimulated nitric oxide production in the retina. Vis Neurosci 17:557

Cao Y, Guo P, Zhao B-L (2005) Simultaneous detection of NO and ROS by ESR in biological system. Method Enzymol 396:77–83

Chandok MR, Ekengren SK, Martin GB, Klessig DF (2004) Suppression of pathogen-inducible NO synthase (iNOS) activity in tomato increases susceptibility to *Pseudomonas syringae*. Proc Natl Acad Sci USA 101:8239–8244

Dangl J (1998) Plants just say NO to pathogens. Nature 394:525–526

Delledonne M, Xia YJ, Dixon RA, Lamb C (1998) Nitric oxide function as a signal in plant disease resistance. Nature 394:585–588

Durner J, Wendohenne D, Klessing DF (1998) Defense gene induction in tobacco by nitric oxide, cyclic ADP-ribose. Proc Natl Acad Sci USA 95:10328–10333

Feng Y, Wang HY, Zhao BL, Lu ZB (2016) Protective effect of a new formula based on nitric oxide and natural antioxidants on myocardium. J Univ Chin Acad Sci 33:625–631

Ferrer MA, Ros Bareclo A (1999) Differential effects of nitric oxide on peroxidase and H_2O_2 production by the xylem of *Zinnia elegans*. Plant Cell Environ 22:891–897

Fu G, Liu W, Li Y, Jin Y, Jiang L, Liang X, Feng S, Dai Z (2014) Magnetic prussian blue nanoparticles for targeted photothermal therapy under magnetic resonance imaging guidance. Bioconjugate Chem 25:1655–1663

Gao M, Zhang J, Zhao BL (2016) Protective effect of nitric oxide and natural antioxidants on stability of blood. Hans journal of food and nutrition. Science 5(1):1–11

Gorbunov NV, Pogue-Geile KL, Epperly MW, Bigbee WL, Draviam R, Day BW, Wald N, Watkins SC, Greenberger JS (2000) Activation of the nitric oxide synthase 2 pathway in the response of bone marrow stromal cells to high doses of ionizing radiation. Radiat Res 154:73–86

Gouvea CMCP, Souza JF, Magalhacs ACN, Martins IS (1997) NO-releasing substance that induce growth elongation in maize root segments. Plant Growth Regul 21:183–187

Guo P, Cao Y-L, Li Z-Q, Zhao B-L (2004) Role of an endogenous nitric oxide burst in the resistance of wheat to stripe rust. Plant Cell Environ 27(4):473–477

Guo SH, Bezard E, Zhao B-L (2005) Protective effect of green tea polyphenols on the SH-SY5Y cells against 6-OHDA induced apoptosis through ROS-NO pathway. Free Radic Biol Med 39:682–695

Hiramatsu M, Oikawa K, Noda H, Mori A, Ogata T, Kamada H (1995) Free radical imaging by electron spin resonance computed tomography in rat brain. Brain Res 697:44–47

Hou H, Khan N, O'Hara JA, Grinberg OY, Dunn JF, Abajian MA, Wilmot CM, Demidenko E, Lu S, Steffen RP, Swartz HM (2005) Increased oxygenation of intracranial tumors by efaproxyn (efaproxiral), an allosteric hemoglobin modifier: *in vivo* EPR oximetry study. Int J Radiat Oncol Biol Phys 61:1503–1509

Itoh Y, Ma FH, Hoshi H, Oka M, Noda K, Ukai Y, Kojima H, Nagano T, Toda N (2000) Determination and bioimaging method for nitric oxide in biological specimens by diaminofluorescein fluorometry. Anal Biochem 287:203–209

Kobayashi H, Watanabe R, Choyke P (2014) Improving conventional enhanced permeability and retention (EPR) effects; what is the appropriate target? Theranostics 4(1):81–89

Kojima H, Hashimoto H, Yoda K (2014) Interaction among the Subunits of Golgi membrane Mannosyltransferase complexes of the yeast. Biosci Biotechnol Biochem 63(11):1970–1976

Kojima H, Nakatsubo N, Kikuchi K, Urano Y, Higuchi T, Tanaka J, Kudo Y, Nagano T (1998a) Direct evidence of NO production in rat hippocampus and cortex using a new fluorescent indicator: DAF-2 DA. NeuroReport 9:3345

Kojima H, Nakatsubo N, Kikuchi K, Kawahara S, Kirino Y, Nagoshi H, Hirata Y, Nagano T (1998b) Detection and imaging of nitric oxide with novel fluorescent indicators: diaminofluoresceins. Anal Chem 70:2446

Kuppusamy P, Chzhan M, Vij K, Shteynbuk M, Lefer DJ, Giannella E, Zweier JL (1994) Three-dimensional spectral-spatial EPR imaging of free radicals in the heart: a technique for imaging tissue metabolism and oxygenation. Proc Natl Acad Sci USA 91:3388–3392

Kuppusamy P, Wang P, Zweier JL (1995a) Three-dimensional spatial EPR imaging of the rat heart. Magn Reson Med 34:99–105

Kuppusamy P, Chzhan M, Zweier JL (1995b) Developement and optimization of three-dimensional spatial EPR imaging for biological organs and tissues. J Magn Reson 106:122–130

Kuppusamy P, Ohnishi ST, Numagami Y, Ohnishi T, Zweier JL (1996) Res Chem Intermed 22:605

Lancaster JR Jr (1994) Simulation of the diffusion and reaction of endogenously produced nitric oxide. Proc Natl Acad Sci USA 91:8137–8141

Laxalt A, Beligni MV, Lamattina L (1997) Nitric oxide preserves the level of chlorophyll in potato leaves infected by *Phytophthora infestans*. Eur J Plant Pathol 73:643–651

Leshem YY, Haramaty E (1996) The charaterization and contrasting effects of the nitricoxide free radical in vegetative stress and senescence of *Pisum sativum* Linn. foliage. J Plant Physiol 148:258–263

Leshem YY, Pinchasov Y (2000) Non-invasive photoacoustic spectroscopic determination of relative endogenous nitric oxide and ethylene content stoichiometry during the ripening of strawberries *Fragaria anannasa* (duch) and avocados *Persea amaricana* (Mill). J Exp Bot 51:1471–1473

Leshem YY, Wills RBH, Ku VVV (1998) Evidence for the function of free radical gas-nitric oxide (NO.) as an endogenous maturation and senescence regulation factor in higher plants. Plant Phys Biochem 36:825–833

Li H-T, Hu J-G, Xin W-J, Zhao B-L (2000) Production and interaction of oxygen and nitric oxide free radicals in PMA stimulated macrophages during the respiratory. Redox Rep 5:353–358

Lin W, Liu J, Jeffries C, Yang L, Lu Y, Lee RE, Chen T (2014) Development of BODIPY FL vindoline as a novel and high-affinity pregnane X receptor fluorescent probe. Bioconjugate Chem 25(9):1664–1677

Lopez-Figueroa MO, Day HEW, River C, Akil H, Watson SJ (2000a) Temporal and anatomical distribution of nitric oxide synthase mRNA expression and nitric oxide production during central nervous system inflammation. Brain Res 852:239–246

Lopez-Figueroa MO, Caamano C, Morano MI, Ronn LC, Akil H, Watson SJ (2000b) Direct evidence of nitric oxide presence within mitochondria. Biochem Biophys Res Commun 272:129

Maeda H (2012) Macromolecular therapeutics in cancer treatment: the EPR effect and beyond. J Control Release 164:138–144

Maeda H (2013) The link between infection and cancer: tumor vasculature, free radicals, and drug delivery to tumors via the EPR effect. Cancer Sci 104:779–789

Matsumoto K, Hyodo F, Matsumoto A, Koretsky AP, Sowers AL, Mitchell JB, Krishna MC (2006) High-resolution mapping of tumor redox status by magnetic resonance imaging using nitroxides as redox-sensitive contrast agents. Clin Cancer Res 12:2455–2462

Mikuni T, He G, Petryakov S, Fallouh MM, Deng Y, Ishihara R, Kuppusamy P, Tatsuta M, Zweier JL (2004) *In vivo* detection of gastric cancer in rats by electron paramagnetic resonance imaging. Cancer Res 64:6495–6502

Millar AH, Day DA (1997) Alternative solution to radical problems. Trend Plant Sci 2:289–290

Morosan DE, Gallagher PT, Zucca P, O'Flannagain A, Fallows R, Reid H, Magdalenic J, Mann G, Bisi MM, Kerdraon A, Konovalenko AA, MacKinnon AL, Rucker HO, Thide B, Vocks C, Alexov A, Anderson J, Asgekar A, Avruch IM, Bentum MJ, Bernardi G, Bonafede A, Breitling F, Broderick JW, Brouw WN, Butcher HR, Ciardi B, de Geus E, Eisloffel J, Falcke H, Frieswijk W, Garrett MA, Griessmeier J, Gunst AW, Hessels JWT, Hoeft M, Karastergiou A, Kondratiev VI, Kuper G, van Leeuwen J,

McKay-Bukowski D, McKean JP, Munk H, Orru E, Paas H, Pizzo R, Polatidis AG, Scaife AMM, Sluman J, Tasse C, Toribio MC, Vermeulen R, Zarka P (2015) LOFAR tied-array imaging and spectroscopy of solar S bursts. Astron. Astrophys 580:A65

Nagano T, Yoshimura T (2002) Bioimaging of nitric oxide. Chem Rev 102:1235–1269

Neill SJ, Desikan R, Hancock JT (2003) Nitric oxide signalling in plants. New Phytol 159:11

Noritake T, Kawakita K, Doke N (1996) Nitric oxide induces phytoalexin accumulation in potato tuber tissue. Plant Cell Physiol 37:113–116

Pedroso MC, Magalhaes JR, Durzan D (2000a) A nitric oxide burst precedes apoptosis in angiosperm and gymnosperm callus cells and foliar tissues. J Exp Bot 51:1027

Pedroso MC, Magalhaes JR, Durzan D (2000b) Nitric oxide induces cell death in *Taxus* cells. Plant Sci 157:173–180

Shen J-G, Wang J, Zhao B-L, Hou J-W, Gao T-L, Xin W-J (1998) Effects of EGb-761 on nitric oxide, oxygen free radicals, myocardial damage and arrhythmias in ischemia-reperfusion injury *in vivo*. Biochim Biophys Acta 1406:228–236

Shen J-G, Li M, Xin W-J, Zhao B-L (2000) Effects of Chinonin on nitric oxide free radical, myocardial damage and arrhythmia in ischemia-reperfusion injury *in vivo*. Appl Magn Reson 19:9–19

Stohr C, Ullrich WR (2002) Generation and possible roles of NO in plant roots and their apoplastic space. J Exp Bot 53:2293

Suzuki Y, Fujii S, Tominaga T, Yoshimoto T, Fujii S, Akaike T, Maeda H, Yoshimura TJ (1999) Direct evidence of *in vivo* nitric oxide production and inducible nitric oxide synthase mRNA expression in the brain of living rat during experimental meningitis. Cereb Blood Flow Metab 19:175

Ueda Y, Yokoyama H, Ohya-Nishiguchi H, Kamada H (1997) ESR Imaging of the rat brain with a nitroxide radical perfused by *in vivo* microdialysis. Magn Reson Imaging 15:355–360

Van Camp W, Inze D, Van Montagu M (1998) H_2O_2 and NO: redox signals in disease resistance. Trends Plant Sci 3:330–334

Velayutham M, Li HH, Kuppusamy P, Zweier JL (2003) Mapping ischemic risk region and necrosis in the isolated heart using EPR imaging. Magn Reson Med 49:1181–1187

Wendehenne D, Pugin A, Klessig DF, Durner J (2001) Nitric oxide: comparative synthesis and signaling in animal and plant cells. Trends Plant Sci 6:177–183

Wink DA, Hanbauer L, Krishna MC, Graeff R, Lee HC, Foster R, Chua N-H (1997) Abscisic acid signaling through cyclic ADP-ribose in plant. Science 282:226–230

Wu K, Huang C, Cong J, Xian H, Wang C, Gao S (2005) Plate form three-dimensional gradient coils for L-band ESR imaging experiment. J Magn Reson 175:256–263

Wu K, Huang C, Cao Y, Zheng Y, Cong J, Xian HG, Wang CN, Gao S, Zhao B-L (2007) Plate form three-dimensional gradient coils for L-band ESR imaging experiment. J Magn Reson 184:357

Xu Y-C, Zhao B-L (2003) The main origin of endogenous NO in higher non-leguminous plant. Plant Physiol Biochem 41:833–838

Xu Y-C, Cao Y-L, Guo P, Zhao B-L (2004) Detection of nitric oxide in plants by electron spin resonance. Phytopath 94:402–407

Xu Y-C, Cao Y-L, Guo P, Zhao B-L (2005) Technique of detection of NO in plants by ESR spin trapping. Method Enzym 396:84–92

Yermolaieva O, Brot N, Weissbach H, Heinemann SH, Hoshi T (2000) Reactive oxygen species and nitric oxide mediate plasticity of neuronal calcium signaling. Proc Natl Acad Sci USA 97:448

Yokoyama H, Yoshimura T, Fujii S, Takayama F, Oikawa K, Kamada H (1996) *In vivo* EPR detection and imaging of endogenous nitric oxide in lipopolysaccharide-treated mice. Nat Biotechnol 14:992–994

Yokoyama H, Fujii S, Yoshimura T, Ohya-Nishiguchi H, Kamada H (1997) *In vivo* ESR–CT imaging of the liver in mice receiving subcutaneous injection of nitric oxide-bound iron complex. Magn Reson Imaging 15:249–253

Yokoyama H, Itoh O, Aoyama M, Obara H, Ohya H, Kamada H (2000) *In vivo* EPR imaging by using an acyl-protected hydroxylamine to analyze intracerebral oxidative stress in rats after epileptic seizures. Magn Reson Imaging 18:875–879

Yokoyama H, Itoh O, Aoyama M, Obara H, Kamada H (2002) *In vivo* temporal EPR imaging of the brain of rats by using two types of blood-brain barrier-permeable nitroxide radicals. Magn Reson Imaging 20:277–284

Yoshimura T, Fujii S, Yokoyama H, Kamada H (1995) *In vivo* electron paramagnetic resonance imaging of NO-bound iron complex in a rat head. Chem Lett 24(4):309–310

Zeidler D, Zähringer U, Gerber I, Dubery I, Hartung T, Bors W, Hutzler P, Durner J (2004) Innate immunity in *Arabidopsis thaliana*: lipopolysaccharides activate nitric oxide synthase (NOS) and induce defense genes. Proc Natl Acad Sci USA 101:15811–15816

Zhang DJ, Xiong J, Hu Y, Li Y, Zhao B (2001) Improved method to detect nitric oxide in biological systems. Appl Magn Reson 20:345–356

Zhang Y-T, Zhang D-L, Cao Y-L, Zhao B-L (2002) Developmental experession and activity variation of nitric oxide synthesase in the brain of golden hamster. Brain Res Bull 58:385–389

Zhang YT, Zhang J, Zhao B-L (2004a) Nitric oxide synthase inhibition prevents neuronal death in the developing visual cortex. Eur J Neurosci 20:2251–2259

Zhang D-L, Yin J-J, Zhao B-L (2004b) Oral administration of *Crataegus* extraction protects against ischemia/reperfusion brain damage in the *Mongolian gerbils*. J Neurochem 90:211–219

Zhao B-L (2005) Nitric oxide in neurodegenarative diseases. Front Biosci 10:454–461

Zhao BL (2015) "Double Edge" effects of nitric oxide free radical in cardio-brain-vascular diseases and health studied by ESR. Chin J Magn Reson 32:195–207

Zhao B-L, Wang J-C, Hou J-W, Xin W-J (1996a) Studies on the mechanism of generation of NO free radicals from polymorphonuclear leukocytes stimulated by PMA. Cell Biol Int Rep 20:343–350

Zhao B-L, Shen J-G, Li M, Xin W-J (1996b) Scavenging effect of Chinonin on NO and oxygen free radicals generated from ischemia reperfusion myocardium. Biochem Biophys Acta 1317:131–137

Zhou GY, Zhao BL, Hou JW, Li MF, Chen C, Xin WJ (1999) Detect of nitric oxide in tissue by spin trapping EPR spectroscopy and triacetylglycerol extraction. Biotechnol Tech 13:507–511

Zou J, Zhang H (2017) Super-resolution reconstruction of color image based on microarray lens. In: 2017 international conference on applied system innovation (ICASI), pp. 830–833

Zweier JL, Chzhan M, Samouilov A (1998) Electron paramagnetic resonance imaging of the rat heart. Phys Med Biol 43:1823–1835

